Journal of Sound and Vibration (2000) **233**(1), 19–40
doi:10.1006/jsvi.1999.2788, available online at http://www.idealibrary.com on IDEAL®

POSTBUCKLING AND VIBRATION CHARACTERISTICS OF PIEZOLAMINATED COMPOSITE PLATE SUBJECT TO THERMO-PIEZOELECTRIC LOADS

I. K. OH, J. H. HAN AND I. LEE

Department of Aerospace Engineering, KAIST 373-1 *Kusong-dong, Yusong-gu, TAEJON* 305-701, *Korea*

(*Received* 8 *July* 1999, *and in final form* 12 *November* 1999)

Postbuckling and vibration analyses considering large thermopiezoelastic deflections are performed for fully symmetric and partially eccentric piezolaminated composite plates. Non-linear finite element equations based on the layerwise displacement theory are formulated for piezolaminated plates subject to thermal piezoelectric loads. The results demonstrate a methodology for raising the thermal buckling temperature and decreasing the thermal postbuckled deflection. Vibration characteristics under complex thermopiezoelectric loads are investigated in the prebuckling and postbuckling regions. For fully distributed piezolaminates, this study shows that excessive bending moments for the suppression of thermally buckled deflection may cause another type of structural instability. In addition, the effective placement of piezoceramic patches is studied to improve suppression of thermally buckled deflection for the partially segmented piezolaminates.

1. INTRODUCTION

On the advent of space shuttle and high-speed aircraft, structures under high-temperature environments have been extensively investigated. Thermal stresses due to solar radiative, aerodynamic and propulsive heating may induce buckling and dynamic instability. Recently, advanced composite materials with high specific stiffness and strength have been widely used for aerospace applications. In addition, smart structure concepts have appeared to enhance structural performance such as buckling and vibration control. Numerous studies on the modelling and analysis of piezolaminated composite structures have been performed. Bailey and Hubbard [1] reported vibration control of a piezoelectric beam with a simplified beam model. Mathematical modellings on piezoeletric composite beams, plates and shells have been performed based on classical and other equivalent single-layer laminate theories by many researchers including Crawley and de Luis [2], Wang and Rogers [3], Hwang and Park [4], Lee [5], Han and Lee [6] Tzou and Gadre [7] and Tzou and Tseng [8]. Recently, discrete layer theories have been utilized for the analyses of composite structures with piezoelectrics in order to fully consider the effects of transverse shear and variable in-plane displacements; see Robbins and Reddy [9], Saravanos and Heyliger [10] and Han and Lee [11].

Skin panels of space shuttles and high-speed vehicles experience large deflections due to thermal postbuckling. Therefore, non-linear analysis is required to consider the large thermally postbuckled deflections. Lee and Lee [12] investigated vibration behaviors of thermally postbuckled anisotropic plates using the first order shear deformable theory. Barbero and Reddy [13] formulated a geometrical non-linear layerwise displacement

0022-460X/00/210019 + 22 $35.00/0

theory to effectively consider the transverse shear effect. Pai *et al.* [14] studied a refined model for non-linear composite plates with piezoelectric layers. Tzou and co-workers [15–17] proposed the mathematical modelling of non-linear thermopiezoelectric laminates and investigated the static and dynamic control of beams and plates. Lee and Saravanos [18] formulated the linear finite element equations for multilayered thermal piezoelectric composite plates with layerwise generalization to capture locally induced piezoelectric and thermal effects.

Numerous modellings and analyses have been performed to investigate induced static deformations, linear bucklings and vibrations of piezolaminated structures. However, the investigations for thermopiezoelectric buckling and postbuckling of composite plates with active piezoelectric layers are still undeveloped areas. To the author's knowledge, the study of thermopiezoelectric postbuckling and vibration of composite plates with the consideration of discrete layer in-plane displacements and geometrical non-linearity has not been performed. In this paper, non-linear finite element equations based on the layerwise plate theory have been formulated for a piezolaminated plate subject to thermal and piezoelectric loads. Also, the postbuckling and vibration characteristics considering large thermopiezoelastic deflections have been analyzed for a square composite plate with fully and partially bonded piezoelectric actuators. The stepped geometry due to partially bonded piezoelectric actuators has been modelled by using different in-plane degrees of freedom per each finite element. The results demonstrated a valid method for raising the thermal buckling temperatures and decreasing the thermal postbuckled deflections. It was also found that the excessive bending moments for the control of postbuckled deflections cause another type of structural instability. The effectiveness of postbuckled deflection control according to configurations of piezoelectric actuators has also been investigated.

2. FORMULATION OF NON-LINEAR FINITE ELEMENT EQUATIONS

2.1. GOVERNING EQUATIONS OF THERMOPIEZOELECTRIC MATERIAL

The linear constitutive equations of a piezoelectric material including the effect of thermal expansion can be written as

$$\sigma_i = Q_{ij}^{E,\Delta T}\varepsilon_j - e_{ki}E_k - \alpha_i^{S,E}\Delta T, \tag{1}$$

$$D_k = e_{kj}\varepsilon_j + \varepsilon_{kl}^{S,\Delta T}E_l + p_k^{S,E}\Delta T, \tag{2}$$

where $i, j = 1, 2, \ldots, 6$ and $k,\ l = 1, 2, 3$; σ_i, ε_j, E_k, D_k and ΔT represent the stress, strain, electric field, electric displacement and temperature rise respectively; $Q_{ij}^{E,\Delta T}$, $\varepsilon_{kl}^{S,\Delta T}$, e_{kj}, $\alpha_i^{S,E}$ and $p_k^{S,E}$ are the elastic moduli, dielectric constant, piezoelectric coefficient, thermal expansion coefficient and temperature stress coefficient respectively. These material constants are measured for constant physical quantities specified by the superscripts. For example, $C_{ij}^{E,\Delta T}$ is measured for zero electric field and zero temperature rise.

For the plate type piezoelectric material, only thickness direction electric field E_3 and electric displacement D_3 are dominant. In addition, the normal stress σ_3 is negligible. After proper co-ordinate transformation, detailed constitutive expressions for the plate type

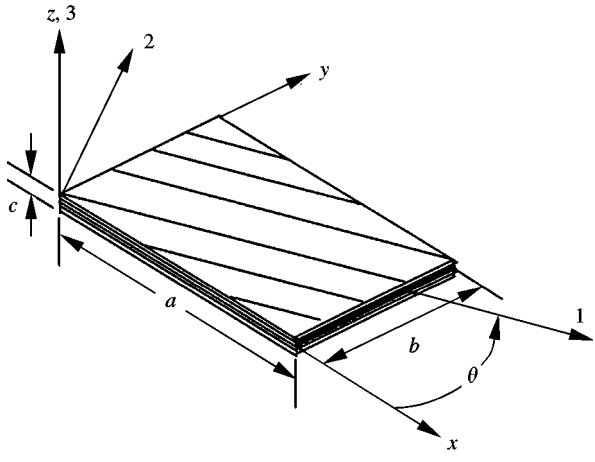

Figure 1. Geometry of laminated composite plate.

piezoelectric material in the geometric co-ordinate can be written as

$$\begin{Bmatrix} \sigma_x \\ \sigma_y \\ \tau_{xy} \\ \tau_{yz} \\ \tau_{xz} \end{Bmatrix} = \begin{bmatrix} \bar{Q}_{11} & \bar{Q}_{12} & \bar{Q}_{16} & 0 & 0 \\ \bar{Q}_{12} & \bar{Q}_{22} & \bar{Q}_{26} & 0 & 0 \\ \bar{Q}_{16} & \bar{Q}_{26} & \bar{Q}_{66} & 0 & 0 \\ 0 & 0 & 0 & \bar{Q}_{44} & \bar{Q}_{45} \\ 0 & 0 & 0 & \bar{Q}_{45} & \bar{Q}_{55} \end{bmatrix}_k \left\{ \begin{Bmatrix} \varepsilon_x \\ \varepsilon_y \\ \gamma_{xy} \\ \gamma_{yz} \\ \gamma_{xz} \end{Bmatrix} - \begin{bmatrix} \alpha_x \\ \alpha_y \\ \alpha_{xy} \\ 0 \\ 0 \end{bmatrix} \Delta T - \begin{bmatrix} d_x \\ d_y \\ d_{xy} \\ 0 \\ 0 \end{bmatrix} E_3 \right\}_k \tag{3}$$

$$= [\bar{Q}]_k (\{\varepsilon\}_k - \{\bar{\alpha}\}_k \Delta T_k - \{\bar{d}\}_k E_3),$$

where subscript k indicates the layer number and $[\bar{Q}]_k$ is the transformed reduced stiffness matrix for the kth composite lamina,

$$[\bar{Q}] = [R]^{-1} [Q] [R]^{-\mathrm{T}}, \tag{4}$$

where

$$[R] = \begin{bmatrix} m^2 & n^2 & 2mn & 0 & 0 \\ n^2 & m^2 & -2mn & 0 & 0 \\ -mn & mn & m^2 - n^2 & 0 & 0 \\ 0 & 0 & 0 & m & -n \\ 0 & 0 & 0 & n & m \end{bmatrix}, \tag{5}$$

and $m = \cos\theta$, $n = \sin\theta$. The fiber angle, θ, is defined in Figure 1. The transformed thermal expansion coefficients and piezoelectric constants are as follows:

$$\begin{Bmatrix} \alpha_x \\ \alpha_y \\ \alpha_{xy} \end{Bmatrix} = \begin{Bmatrix} m^2\alpha_1 + n^2\alpha_2 \\ n^2\alpha_1 + m^2\alpha_2 \\ 2mn(\alpha_1 - \alpha_2) \end{Bmatrix}, \qquad \begin{Bmatrix} d_x \\ d_y \\ d_{xy} \end{Bmatrix} = \begin{Bmatrix} m^2 d_1 + n^2 d_2 \\ n^2 d_1 + m^2 d_2 \\ 2mn(d_1 - d_2) \end{Bmatrix}. \tag{6}$$

2.2. LAYERWISE LAMINATED THEORY WITH GEOMETRIC NON-LINEARITY

Based on the layerwise plate theory [13], the displacement fields (u, v and w) for a two-dimensional element i, of which the area is defined as Ω_i, can be expressed by introducing the following piecewise continuous approximations shown in Figure 2:

$$u(x, y, z, t) = \sum_{J=1}^{N_i} U^J(x, y, t)\,\Phi^J(z),$$

$$v(x, y, z, t) = \sum_{J=1}^{N_i} V^J(x, y, t)\,\Phi^J(z), \tag{7}$$

$$w(x, y, z, t) = W(x, y, t),$$

where U^J and V^J are in-plane displacements at the Jth interface; N_i is the number of degrees of freedom for the in-plane displacement along the thickness direction for the element i; $\Phi^J(z)$ is the Lagrangian interpolation function and assumed to be of the following form:

$$\Phi^J(z) = \begin{cases} 0 & \text{for } z < z_{J-1}, \\ \Psi_2^{J-1}(z) = \dfrac{z - z_{J-1}}{z_J - z_{J-1}} & \text{for } z_{J-1} < z < z_J, \\ \Psi_1^J(z) = \dfrac{z - z_{J+1}}{z_{J+1} - z_J} & \text{for } z_J < z < z_{J+1}, \\ 0 & \text{for } z_{J+1} < z, \end{cases} \tag{8}$$

where z_J denotes the global thickness co-ordinate of the Jth interface. Note that the stepped geometry of piezolaminated plates can be properly modelled by assigning different numbers to N_i for each two-dimensional element.

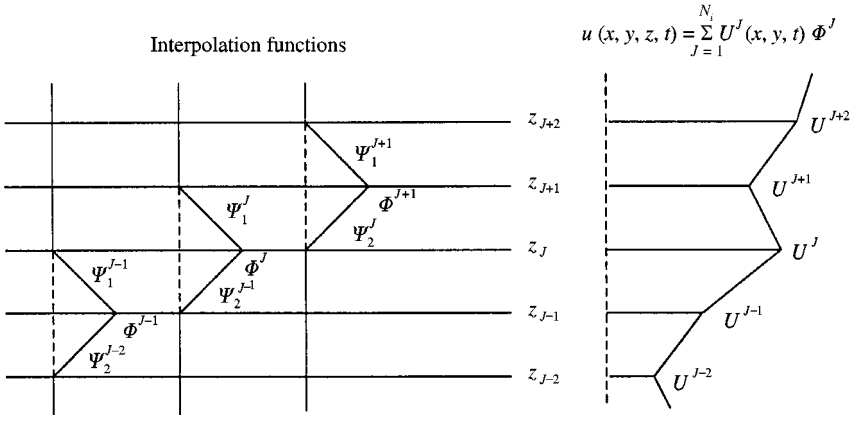

Figure 2. In-plane displacement field based on layerwise theory.

The von Karman non-linear strain displacement relation is adopted to consider a large deflection due to the thermal and piezoelectric loads. The strain-displacement relationships can be written as follows:

$$\varepsilon_x = \frac{\partial u}{\partial x} + \frac{1}{2}\left(\frac{\partial w}{\partial x}\right)^2 = \sum_{J=1}^{N_i} \frac{\partial U^J}{\partial x} \Phi^J + \frac{1}{2}\left(\frac{\partial W}{\partial x}\right)^2, \tag{9a}$$

$$\varepsilon_y = \frac{\partial v}{\partial y} + \frac{1}{2}\left(\frac{\partial w}{\partial y}\right)^2 = \sum_{J=1}^{N_i} \frac{\partial V^J}{\partial y} \Phi^J + \frac{1}{2}\left(\frac{\partial W}{\partial y}\right)^2, \tag{9b}$$

$$\gamma_{xy} = \frac{\partial u}{\partial y} + \frac{\partial v}{\partial x} + \frac{\partial w}{\partial x}\frac{\partial w}{\partial y} = \sum_{J=1}^{N_i} \left(\frac{\partial U^J}{\partial y} + \frac{\partial V^J}{\partial x}\right)\Phi^J + \frac{\partial W}{\partial x}\frac{\partial W}{\partial y}, \tag{9c}$$

$$\gamma_{yz} = \frac{\partial w}{\partial y} + \frac{\partial v}{\partial z} = \frac{\partial W}{\partial y} + \sum_{J=1}^{N_i} V^J \frac{\mathrm{d}\Phi^J}{\mathrm{d}z}, \tag{9d}$$

$$\gamma_{xz} = \frac{\partial w}{\partial x} + \frac{\partial u}{\partial z} = \frac{\partial W}{\partial x} + \sum_{J=1}^{N_i} U^J \frac{\mathrm{d}\Phi^J}{\mathrm{d}z}. \tag{9e}$$

2.3. HAMILTON'S PRINCIPLES

In order to derive the equation of motion for the thermopiezoelastic composite plate, Hamilton's principle was applied. The equations of motion can be expressed as follows:

$$\int_0^{\mathrm{T}} \int_{\Omega_i} \Bigg[\sum_{J=1}^{N_i} \left(N_x^J \frac{\partial \delta U^J}{\partial x} + N_y^J \frac{\partial \delta V^J}{\partial y} + N_{xy}^J \left(\frac{\partial \delta U^J}{\partial y} + \frac{\partial \delta V^J}{\partial x} \right) + Q_y^J \delta V^J + Q_x^J \delta U^J \right)$$
$$+ Q_y \frac{\partial \delta W}{\partial y} + Q_x \frac{\partial \delta W}{\partial x} + N_x \frac{\partial W}{\partial x}\frac{\partial \delta W}{\partial x} + N_y \frac{\partial W}{\partial y}\frac{\partial \delta W}{\partial y} + N_{xy}\left(\frac{\partial W}{\partial x}\frac{\partial \delta W}{\partial y} + \frac{\partial \delta W}{\partial x}\frac{\partial W}{\partial y} \right)$$
$$+ \sum_{J=1}^{N_i} \sum_{K=1}^{N_i} I^{JK} (\ddot{U}^J \delta U^K + \ddot{V}^J \delta V^K) + I^0 \ddot{W} \delta W \Bigg] \mathrm{d}A \, \mathrm{d}t = 0, \tag{10}$$

where

$$\mathbf{Q} = \{Q_y \;\; Q_x\}^{\mathrm{T}} = \mathbf{A}_S \mathbf{e} + \sum_{J=1}^{N_i} \mathbf{B}_S^J \mathbf{e}_S^J, \tag{11a}$$

$$\mathbf{N} = \{N_x \;\; N_y \;\; N_{xy}\}^{\mathrm{T}} = \mathbf{A}\frac{1}{2}\mathbf{G}\tilde{\mathbf{e}} + \sum_{J=1}^{N_i} \mathbf{B}^J \mathbf{e}^J - \{N_{\Delta T}\} - \{N_P\}, \tag{11b}$$

$$\mathbf{N}^J = \{N_x^J \;\; N_y^J \;\; N_{xy}^J\}^{\mathrm{T}} = \sum_{K=1}^{N_i} \left(\mathbf{B}^J \frac{1}{2} \mathbf{G}\tilde{\mathbf{e}} + \mathbf{D}^{JK} \mathbf{e}^K - \mathbf{N}_{\Delta T}^J - \mathbf{N}_P^J \right), \tag{11c}$$

$$\mathbf{Q}^J = \{Q_y^J \;\; Q_x^J\}^{\mathrm{T}} = \mathbf{B}_S^J \mathbf{e} + \sum_{J=1}^{N_i} \mathbf{D}_S^{JK} \mathbf{e}_S^K. \tag{11d}$$

By substituting equation (11) into equation (10), the following variational form is obtained:

$$\int_0^T \int_{\Omega_i} \Bigg[\delta \mathbf{e}^T \mathbf{A}_S \mathbf{e} + \sum_J^{N_i} \{ \delta \mathbf{e}^T \mathbf{B}_S^J \mathbf{e}_S^J + \delta \mathbf{e}_S^{J^T} \mathbf{B}_S^J \mathbf{e} \} + \sum_J^{N_i} \sum_K^{N_i} \{ \delta \mathbf{e}^{J^T} \mathbf{D}^{JK} \mathbf{e}^K + \delta \mathbf{e}_S^{J^T} \mathbf{D}_S^{JK} \mathbf{e}_S^K \}$$

$$+ \frac{1}{2} \sum_J^{N_i} \delta \mathbf{e}^{J^T} \mathbf{B}^{J^T} \mathbf{G} \tilde{\mathbf{e}} + \frac{1}{2} \delta \tilde{\mathbf{e}}^T \mathbf{G}^T \sum_J^{N_i} \mathbf{B}^J \mathbf{e}^J + \frac{1}{2} \delta \tilde{\mathbf{e}}^T \mathbf{N1} \tilde{\mathbf{e}} + \frac{1}{3} \cdot \frac{3}{2} \delta \tilde{\mathbf{e}}^T \mathbf{G}^T \mathbf{A} \mathbf{G} \tilde{\mathbf{e}}$$

$$- \sum_J^{N_i} \delta \mathbf{e}^{J^T} \mathbf{N}_{\Delta T}^J - \sum_J^{N_i} \delta \mathbf{e}^{J^T} \mathbf{N}_P^J - \delta \tilde{\mathbf{e}}^T \mathbf{N}_{\Delta T} \tilde{\mathbf{e}} - \delta \tilde{\mathbf{e}}^T \mathbf{N}_P \tilde{\mathbf{e}}$$

$$+ I^0 \delta W \ddot{W} + \sum_J^{N_i} \sum_K^{N_i} \delta \mathbf{d}^{J^T} \mathbf{I}^{JK} \ddot{\mathbf{d}}^K \Bigg] \mathrm{d}A \, \mathrm{d}t = 0 \tag{12}$$

where subscript S denotes transverse shear properties, and other symbols are defined as follows:

$$\mathbf{e} = \left\{ \frac{\partial W}{\partial y} \; \frac{\partial W}{\partial x} \right\}^T, \quad \tilde{\mathbf{e}} = \left\{ \frac{\partial W}{\partial x} \; \frac{\partial W}{\partial y} \right\}^T, \quad G = \begin{bmatrix} \dfrac{\partial W}{\partial x} & 0 & \dfrac{\partial W}{\partial y} \\ 0 & \dfrac{\partial W}{\partial y} & \dfrac{\partial W}{\partial x} \end{bmatrix}^T, \tag{13a}$$

$$\mathbf{e}_S^J = \{ V^J \;\; U^J \}^T, \quad \mathbf{d}^J = \{ U^J \;\; V^J \}^T, \quad \mathbf{e}^J = \left\{ \frac{\partial U^J}{\partial x} \frac{\partial V^J}{\partial y} \frac{\partial U^J}{\partial y} + \frac{\partial V^J}{\partial x} \right\}^T \tag{13b}$$

and

$$A_{pq} = \int \bar{Q}_{pq} \mathrm{d}z \quad (p, q = 1, 2, 6), \tag{14a}$$

$$A_{S_{pq}} = \int \bar{Q}_{pq} \mathrm{d}z \quad (p, q = 4, 5), \tag{14b}$$

$$B_{pq}^J = \int \bar{Q}_{pq} \frac{\mathrm{d}\Phi^J(z)}{\mathrm{d}z} \mathrm{d}z \quad (p, q = 1, 2, 6), \tag{14c}$$

$$B_{S_{pq}}^J = \int \bar{Q}_{pq} \frac{\mathrm{d}\Phi^J(z)}{\mathrm{d}z} \mathrm{d}z \quad (p, q = 4, 5), \tag{14d}$$

$$D_{pq}^{JK} = \int \bar{Q}_{pq} \Phi^J(z) \Phi^K(z) \mathrm{d}z \quad (p, q = 1, 2, 6), \tag{14e}$$

$$D_{S_{pq}}^{JK} = \int \bar{Q}_{pq} \frac{\mathrm{d}\Phi^J(z)}{\mathrm{d}z} \frac{\mathrm{d}\Phi^K(z)}{\mathrm{d}z} \quad (p, q = 4, 5), \tag{14f}$$

$$(\{N_{\Delta T}\}, \{N_P\}) = \int \bar{Q}_{pq}(\{\bar{\alpha}\}_k \Delta T_k, \{\bar{d}\}_k (V/t^{act})_k) \mathrm{d}z \quad (p, q = 1, 2, 6), \tag{14g}$$

$$(\mathbf{N}^J_{\Delta T}, \mathbf{N}^J_P) = \int \bar{Q}_{pq} \Phi^J(\{\bar{\alpha}\}_k \Delta T_k, \{\bar{d}\}_k (V/t^{act})_k) \mathrm{d}z \quad (p, q = 1, 2, 6), \tag{14h}$$

$$\mathbf{N}_{\Delta T(P)} \begin{bmatrix} N_{\Delta T(P)} x & N_{\Delta T(P)} xy \\ N_{\Delta T(P)} xy & N_{\Delta T(P)} y \end{bmatrix}, \tag{14i}$$

$$\mathbf{N1} = \begin{bmatrix} N1x & N1xy \\ N1xy & N1y \end{bmatrix}, \quad \begin{Bmatrix} N1x \\ N1y \\ N1xy \end{Bmatrix} = \sum_J^{N_i} \mathbf{B}^j \mathbf{e}^J, \tag{14j}$$

$$\mathbf{I}^{JK} = diag(I^{JK}, I^{JK}), \tag{14k}$$

$$(I^0, I^{JK}) = \int_t \rho(1, \Phi^J(z) \Phi^K(z)) \mathrm{d}z. \tag{14l}$$

2.4. FINITE ELEMENT FORMULATION

Over each finite element Ω_i, the displacements are expressed as a linear combination of shape functions $\bar{\psi}_k$ and nodal values W_k, U^J_k, V^J_k as follows:

$$(W, U^J, V^J) = \sum_{k=1}^{NPE} (W_k, U^J_k, V^J_k) \bar{\psi}_k, \tag{15}$$

where NPE is the number of nodes per element. The shape functions used here are 4- and 9-node Lagrangian interpolation with C^0 continuity. Let us define the nodal displacement vector for element i as

$$\mathbf{u}_e = \{(W_1 W_2 \cdots W_{NPE}) \cdots (U^J_1 U^J_2 \cdots U^J_{NPE} V^J_1 V^J_2 \cdots V^J_{NPE}) \cdots\}^{\mathrm{T}}. \tag{16}$$

By substituting equation (15) into equation (12), we can obtain the finite element equation of motion:

$$\mathbf{M}_e \ddot{\mathbf{u}}_e + \mathbf{K}_e \mathbf{u}_e = \mathbf{F}_e. \tag{17}$$

The element mass, stiffness, and force vector can be written as

$$\mathbf{M}_e = \int_{\Omega_i} \begin{bmatrix} I^0 \mathbf{g}^{\mathrm{T}} \mathbf{g} & \cdots & \mathbf{0} & \cdots \\ \vdots & \ddots & & \\ \mathbf{0} & & I^{IJ} \mathbf{G}^{\mathrm{T}}_2 \mathbf{G}_2 & \\ \vdots & & & \ddots \end{bmatrix} \mathrm{d}A, \tag{18a}$$

$$\mathbf{K}_e = \int_{\Omega_i} \begin{bmatrix} \mathbf{H}_1^T \mathbf{A}_S \mathbf{H}_1 - \mathbf{H}_3^{\mathrm{T}}(\mathbf{N}_{\Delta T} + \mathbf{N}_P)\mathbf{H}_3 & & \\ & & \mathbf{H}_1^{\mathrm{T}} \mathbf{B}_S^J \mathbf{G}_1 \\ + \tfrac{1}{2}\mathbf{H}_3^{\mathrm{T}} \mathbf{N1} \mathbf{H}_3 & \cdots & \cdots \\ & & + \tfrac{1}{2}\mathbf{H}_3^{\mathrm{T}} \mathbf{G}^{\mathrm{T}} \mathbf{B}^J \mathbf{H}_2 \\ + \tfrac{1}{3}\tfrac{3}{2}\mathbf{H}_3^{\mathrm{T}} \mathbf{G}^{\mathrm{T}} \mathbf{A} \mathbf{G} \mathbf{H}_3 & & \\ \vdots & \ddots & \\ \mathbf{G}_1^{\mathrm{T}} \mathbf{B}_S^{\mathrm{I}} \mathbf{H}_1 & & \mathbf{H}_2^{\mathrm{T}} \mathbf{D}^{IJ} \mathbf{H}_2 \\ + \tfrac{1}{2}\mathbf{H}_2^{\mathrm{T}} \mathbf{B}^I \mathbf{G} \mathbf{H}_3 & & + \mathbf{G}_1^{\mathrm{T}} \mathbf{D}_S^{IJ} \mathbf{G}_1 \\ \vdots & & \ddots \end{bmatrix} \mathrm{d}A, \quad (18b)$$

$$\mathbf{F}_e = \int_{\Omega_i} \{\mathbf{0} \quad \cdots \quad \mathbf{H}_2^{\mathrm{T}}(\mathbf{N}_{\Delta T}^J + \mathbf{N}_P^J) \quad \cdots\}^{\mathrm{T}} \mathrm{d}A, \quad (18c)$$

where

$$\mathbf{H}_1 = \begin{bmatrix} \mathbf{h}_{\mathrm{y}} \\ \mathbf{h}_{\mathrm{x}} \end{bmatrix}, \quad \mathbf{H}_2 = \begin{bmatrix} \mathbf{h}_{\mathrm{x}} & \mathbf{0} \\ \mathbf{0} & \mathbf{h}_{\mathrm{y}} \\ \mathbf{h}_{\mathrm{y}} & \mathbf{h}_{\mathrm{x}} \end{bmatrix}, \quad \mathbf{H}_3 = \begin{bmatrix} \mathbf{h}_{\mathrm{x}} \\ \mathbf{h}_{\mathrm{y}} \end{bmatrix}, \quad (19a)$$

$$\mathbf{G}_1 = \begin{bmatrix} \mathbf{0} & \mathbf{g}^{\mathrm{T}} \\ \mathbf{g}^{\mathrm{T}} & \mathbf{0} \end{bmatrix}, \qquad \mathbf{G}_2 = \begin{bmatrix} \mathbf{g}^{\mathrm{T}} & \mathbf{0} \\ \mathbf{0} & \mathbf{g}^{\mathrm{T}} \end{bmatrix}, \quad (19b)$$

and

$$\mathbf{h}_{\mathrm{x}} = \left\{ \frac{\partial \bar{\psi}_1}{\partial x} \frac{\partial \bar{\psi}_2}{\partial x} \quad \cdots \frac{\partial \bar{\psi}_{NPE}}{\partial x} \right\}, \quad (19c)$$

$$\mathbf{h}_{\mathrm{y}} = \left\{ \frac{\partial \bar{\psi}_1}{\partial y} \frac{\partial \bar{\psi}_2}{\partial y} \quad \cdots \frac{\partial \bar{\psi}_{NPE}}{\partial y} \right\}, \quad (19d)$$

$$\mathbf{g} = \{\bar{\psi}_1 \quad \bar{\psi}_2 \quad \cdots \quad \bar{\psi}_{NPE}\}^{\mathrm{T}}, \quad (19e)$$

$$\mathbf{0} = \{\overbrace{0 \; 0 \quad \cdots \quad 0}^{NPE}\}^{\mathrm{T}}. \quad (19f)$$

The stiffness matrix term in equation (17) can be partitioned as follows:

$$\mathbf{M}_e \ddot{\mathbf{u}}_e + (\mathbf{K0}_e - \mathbf{K}_e^{\Delta T} - \mathbf{K}_e^P + \tfrac{1}{2}\mathbf{KN1}_e + \tfrac{1}{3}\mathbf{KN2}_e)\mathbf{u}_e = \mathbf{F}_e, \quad (20)$$

where $\mathbf{M}_e$, $\mathbf{K0}_e$, $\mathbf{K}_e^{\Delta T}$, $\mathbf{K}_e^P$, $\mathbf{KN1}_e$, $\mathbf{KN2}_e$ and $\mathbf{F}_e$ are mass matrix, linear stiffness, thermal geometric stiffness, piezoelectric geometric stiffness, first order non-linear stiffness, second order non-linear stiffness and loading vector respectively.

2.5. SOLUTION PROCEDURE OF NON-LINEAR SYSTEM EQUATION

Through the assembly procedure, global finite element equation can be obtained as follows:

$$\mathbf{M}\ddot{\mathbf{u}} + (\mathbf{K0} - \mathbf{K}^{\Delta T} - \mathbf{K}^{P} + \tfrac{1}{2}\mathbf{KN1} + \tfrac{1}{3}\mathbf{KN2})\mathbf{u} = \mathbf{F}. \tag{21}$$

To analyze the thermopiezoelastic postbuckling and vibration of buckled plates, the solution of equation (21) is assumed to be the sum of a time-dependent and a time-independent solution such as $\mathbf{u} = \mathbf{u}_s + \mathbf{u}_t$, where $\mathbf{u}_s$ is the postbuckled deflection and $\mathbf{u}_t$ is the time-dependent solution with small amplitude. Substituting this assumed solution into equation (21), we can obtain static and dynamic coupled equations:

$$(\mathbf{K0} - \mathbf{K}^{\Delta T} - \mathbf{K}^{P} + \tfrac{1}{2}\mathbf{KN1}(\mathbf{u}_s) + \tfrac{1}{3}\mathbf{KN2}(\mathbf{u}_s))\mathbf{u}_s = \mathbf{F}, \tag{22}$$

$$\mathbf{M}\ddot{\mathbf{u}}_t + (\mathbf{K0} - \mathbf{K}^{\Delta T} - \mathbf{K}^{P} + \mathbf{KN1}(\mathbf{u}_s) + \mathbf{KN2}(\mathbf{u}_s))\mathbf{u}_t = \mathbf{0}. \tag{23}$$

First thermal Euler buckling analysis is performed to find the reference buckling temperature rise,

$$(\mathbf{K0} - \Delta T_{cr}\mathbf{K}_0^{\Delta T})\{\Theta\} = \mathbf{0}, \tag{24}$$

where $\mathbf{K}_0^{\Delta T}$ is the geometric stiffness in the state of unit uniform temperature distribution, ΔT_{cr} is critical buckling temperature and $\{\Theta\}$ is the buckling mode. The buckling mode shape is properly scaled to be used as an initial estimated deflection for construction of the non-linear stiffness matrix at postbuckled range.

The Newton–Raphson iteration method is used to solve the non-linear equation (22). For the ith iteration, equation (22) can be written as an incremental equation as follows:

$$(\mathbf{K0} - \mathbf{K}^{\Delta T} - \mathbf{K}^{P} + \mathbf{KN1}(\mathbf{u}_s^i) + \mathbf{KN2}(\mathbf{u}_s^i))\Delta\mathbf{u}_s^{i+1} = \Delta\mathbf{F}^i, \tag{25}$$

where

$$\Delta\mathbf{F}^i = \mathbf{F} - (\mathbf{K0} - \mathbf{K}^{\Delta T} - \mathbf{K}^{P} + \tfrac{1}{2}\mathbf{KN1}(\mathbf{u}_s^i) + \tfrac{1}{3}\mathbf{KN2}(\mathbf{u}_s^i))\mathbf{u}_s^i. \tag{26}$$

By solving equation (25), the updated displacement vector is determined as:

$$\mathbf{u}_s^{i+1} = \mathbf{u}_s^i + \Delta\mathbf{u}_s^{i+1}, \tag{27}$$

where $\mathbf{u}_s^{i+1}$ and $\Delta\mathbf{u}_s^{i+1}$ are static and incremental displacement in the $(i+1)$th iteration.

After obtaining the converged postbuckling deflection, the vibration analysis of thermopiezoelectrically buckled plates can be performed by solving equation (23) as a generalized eigenvalue problem as follows:

$$[\mathbf{K0} - \mathbf{K}^{\Delta T} - \mathbf{K}^{P} + \mathbf{KN1}(\mathbf{u}_s) + \mathbf{KN2}(\mathbf{u}_s) - \omega^2\mathbf{M}]\{\Theta\} = \mathbf{0}. \tag{28}$$

3. RESULTS AND DISCUSSION

3.1. VERIFICATION OF FE CODE

In order to validate the present non-linear layerwise FE code, thermal buckling, postbuckling and piezoelectric transverse deflection have been analyzed and compared with published results. For the first problem, thermal buckling temperatures for isotropic and composite plates have been compared with the results of Gowda and Pandalai [19] and Thangaratnam *et al.* [20]. The critical temperature rise of isotropic square plates with all simply supported and clamped edges subjected to constant temperature distribution has been calculated and compared with previous results in Table 1. Thermal buckling of a composite plate is compared with the results of Thangaratnam *et al.* [20] in Figure 3. The material properties and geometry for thermal buckling of composite plate are

$$E_1/E_2 = 20{\cdot}0, \quad G_{12}/E_2 = 0{\cdot}5,$$

$$\alpha_2/\alpha_1 = 2{\cdot}0, \quad \alpha_1 = 0{\cdot}1 \times 10^{-5}/^{\circ}\mathrm{C} \tag{29}$$

$$a/c = 100{\cdot}0, \quad a/b = 1{\cdot}0.$$

Here, LWPT, FSDT, SSSS BC and CCCC BC are layerwise plate theory, first order shear deformable theory, all simply supported boundary condition and all clamped boundary condition, respectively. The present FSDT results were obtained by using the code developed in reference [12]. The present LWPT results of thermal buckling are in good agreement with those in the literature.

For the second example, postubuckling results are compared with the results of Averil and Reddy [21] in Figure 4. The thickness of each layer was 0·127 mm and the planar dimension of the square plate was 0·15 m. The material properties and SSSS boundary conditions are as follows:

Material properties

$$E_1 = 155\,\mathrm{GPa}, \quad E_2 = E_3 = 8{\cdot}07\,\mathrm{GPa},$$

$$G_{23} = 3{\cdot}25\,\mathrm{GPa}, \quad G_{13} = G_{12} = 4{\cdot}55\,\mathrm{GPa}, \tag{30a}$$

$$\alpha_1 = -0{\cdot}07 \times 10^{-6}/^{\circ}\mathrm{C}, \quad \alpha_2 = \alpha_3 = 30 \times 10^{-6}/^{\circ}\mathrm{C}.$$

TABLE 1

Verification of critical temperature for isotropic square plates ($a/c = 100$, $\alpha = 2 \times 10^{-6}$, $v = 0{\cdot}3$)

Uniform temperature rise	Simply supported BC	Clamped BC
Analytical [19]	63·27	168·71
FEM [20]	63·33	167·70
Present (Mesh† 6×6)	62·33	167·88
Present (Mesh† 7×7)	62·51	167·72

† The 9-node elements are used in the present analysis.

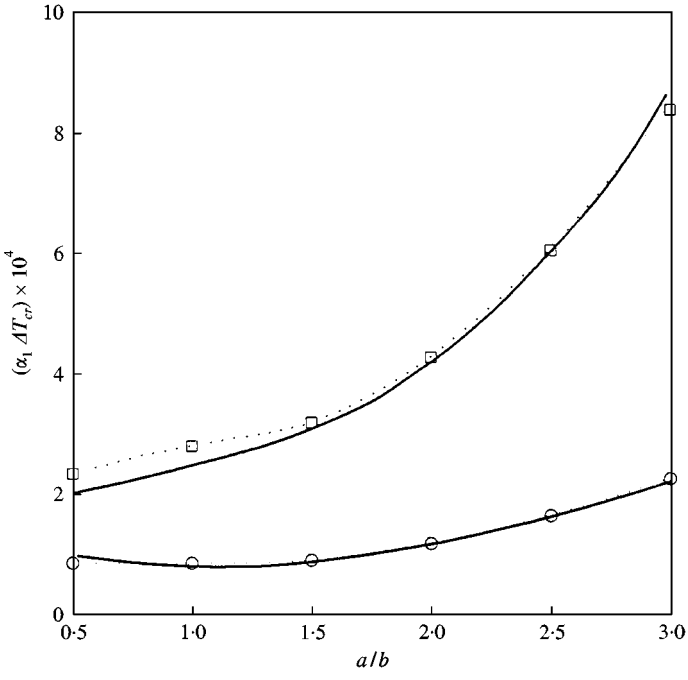

Figure 3. Verification of thermal buckling of symmetric cross-ply laminated plate versus aspect ratio: ——, Thangaratnam *et al.*; ···· present (FSDT); ○, present (LWPT, SSSS BC); □, present (LWPT, CCCC BC).

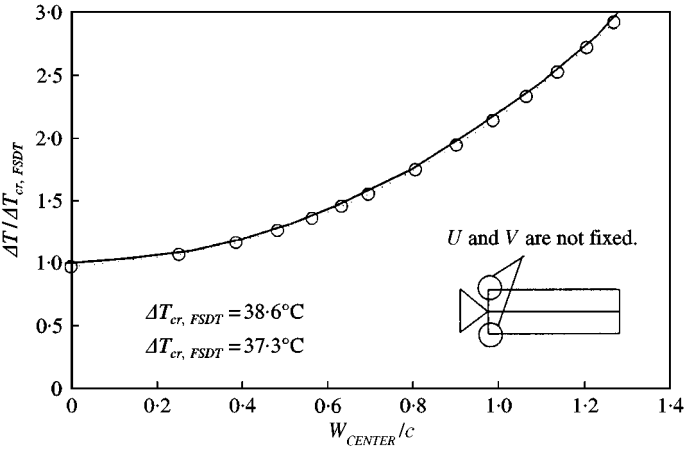

Figure 4. Verification of thermal postbuckling for [0/ ± 45/90]s composite plates: ——, Averill and Reddy (FSDT); ··· ○ ···, present (LWPT).

SSSS boundary conditions in LWPT:

$$W = U^m = 0 \quad \text{at } x = 0, a,$$
$$W = V^m = 0 \quad \text{at } y = 0, b, \tag{30b}$$

where m is in-plane interface at the mid-plane of the composite plate. The normalized center deflection of the plate due to changes in temperature is presented in Figure 4. Because U^J

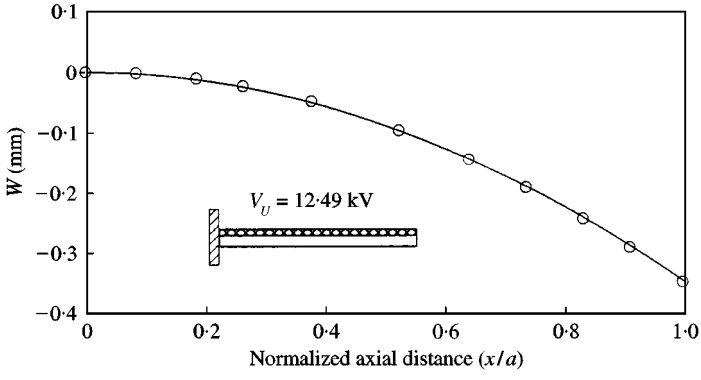

Figure 5. Verification of static deflection for the active beam subject to piezoelectric load: —⊖—, Saravanos; ——, present.

and V^J except the mid-plane is free in the simply supported boundary condition of the present analysis, the present buckling temperature rise is slightly lower than that of Averil and Reddy [21], which was based on the first order shear deformable plate theory. However, the present results of buckling and postbuckling are in good agreement with those of Averil and Reddy [21].

For the last example, the piezoelectric transverse deflection of a three-layer active beam has been analyzed and compared with the results by Saravanos [10]. When the electric potential 12·49 kV is applied between the upper and lower electrodes of the PZT-4 layer, transverse deflection of the active beam is presented in Figure 5. Excellent agreement can be observed in Figure 5 between the present results and Saravanos's results.

3.2. THERMAL POSTBUCKLING OF ISOTROPIC STEPPED PLATE

Thermal postbuckling analyses of both symmetrically and eccentrically stepped isotropic plates with all simply supported boundaries have been performed. The results help to explain the behavior of stepped plates subject to thermal loads. The thick part is located in the center of the plate. The geometry shown in Figure 6 and finite element parameters are as follows:

$$\text{Isotropic material with the Poison ratio } v = 0{\cdot}33, \tag{31a}$$

$$\text{Base plate geometry: } a/b = 1,\ a/c_{BASE} = 100,\ a = 1\,\text{m},\ NIID = 3, \tag{31b}$$

$$\text{Stepped geometry: } a_s/b_s = 1,\ a/a_s = 2,\ c_{BASE}/c_s = 0{\cdot}5,\ NIID = 5, \tag{31c}$$

$$\text{Mesh: } 8 \times 8 \text{ with 9 node elements}, \tag{31d}$$

where NIID denotes the number of degrees of freedom for in-plane displacement. Figure 6 shows the thermal buckling and pustbuckling behavior of symmetrically and eccentrically stepped plates subject to a uniform thermal load. The symmetrically stepped plate shows bifurcation buckling. In the case of the eccentrically stepped plate, transverse deflection exists at a low-temperature rise without bifurcation buckling. At the same temperature field,

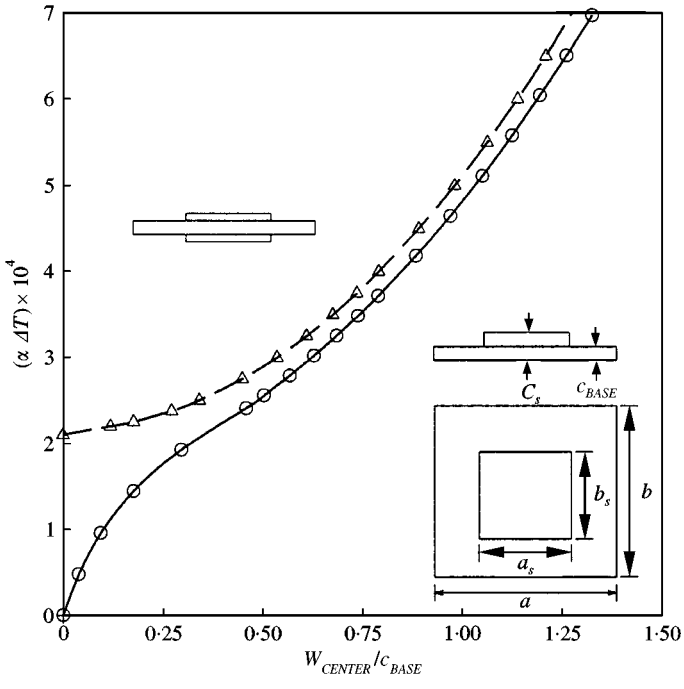

Figure 6. Thermal postbuckling of isotropic stepped plate: —△—, symmetric plate; —○—, eccentric plate.

postbuckled deflection of the eccentrically stepped plate is larger than that of the symmetrically stepped plate. Figure 7 shows the results of a vibration analysis considering postbuckled deflection. In the case of the symmetrically stepped plate, the fundamental frequency approaches zero at the bifurcation buckling point. The frequencies for (1,1) and (1,2) mode of eccentrically stepped plate are higher than that of the symmetrically stepped plate. But, as the thermal load is increased, the frequencies of (2,2) and (1,3) mode of symmetrically stepped plate become higher than those of the eccentrically stepped plate.

3.3. THERMOPIEZOELASTIC POSTBUCKLING OF A SYMMETRICALLY PIEZOLAMINATED PLATE

Thermopiezoelastic postbuckling and vibration analyses are performed for the composite plate with symmetrically fully covered piezoelectric material. Temperature distribution is quasi-steady and uniform in the thickness direction. Table 2 shows the material properties used for this study. The lamination of the piezolaminated composite plate is $[P/0/\pm 45/90]$s, and all boundaries are simply supported. The thickness of graphite/epoxy and piezoceramic is 0·125 and 0·1 mm per lamina respectively. The geometry and finite element parameters are given as follows:

$$\text{Base composite plate geometry: } a/b = 1,\ a/c_{BASE} = 120,\ a = 120\ \text{mm}, \tag{32a}$$

$$\text{Fully covered piezolaminated elements: } c/c_{BASE} = 1{\cdot}2, \tag{32b}$$

$$\text{Mesh: } 12 \times 12 \text{ with 4 node elements.} \tag{32c}$$

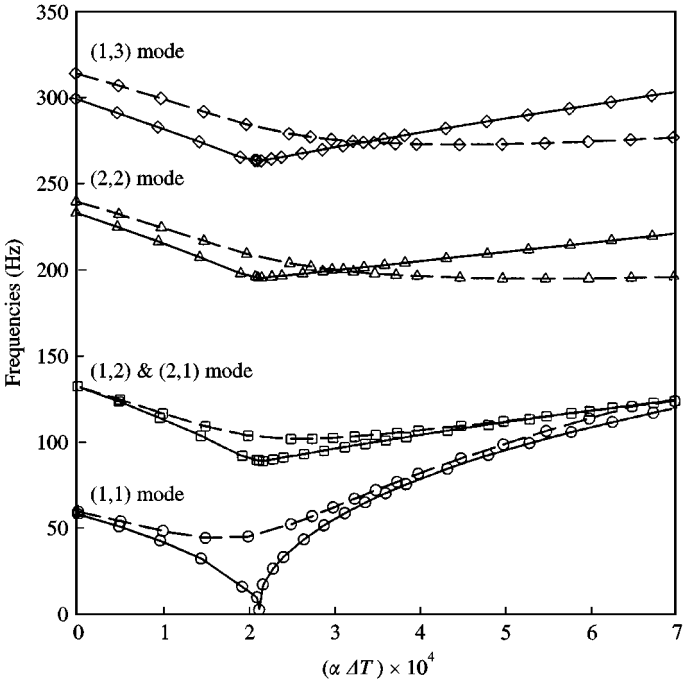

Figure 7. Natural frequencies of isotropic stepped plate subject to thermal loads: – – –, eccentric plate; ——, symmetric plate.

TABLE 2

Material properties of the graphite-epoxy and PZT-5A layers

Properties	Graphite-epoxy	PZT-5A
E_1 (GPa)	150	63
E_2 (GPa)	9·0	63
G_{12} (GPa)	7·1	24·2
G_{23} (GPa)	2·5	24·2
v_{12}	0·3	0·3
α_1 (10^{-6}/°C)	1·1	0·9
α_2 (10^{-6}/°C)	25·2	0·9
d_{31} (10^{-12} m/V)	0	254
d_{32} (10^{-12} m/V)	0	254
ρ (kg/m^3)	1600	7600

When the control voltage with the same sign is applied to both upper and lower piezoceramics, the behavior of thermopiezoelastic buckling and postbuckling is presented in Figure 8. Here, $\Delta T_{cr,G}$ means the thermal buckling temperature rise under a grounding condition. The minus control voltages $V_U = V_L = -100$ V make the plate contract so that the buckling temperature is increased and the postbuckled deflection is decreased at the same temperature rise. In contrast, the plus control voltages decrease the buckling temperature and induce more large postbuckled deflections.

The vibration characteristics of thermopiezoelectrically buckled composite plate are shown in Figure 9. At the buckling point, the fundamental frequencies approach zero. At the

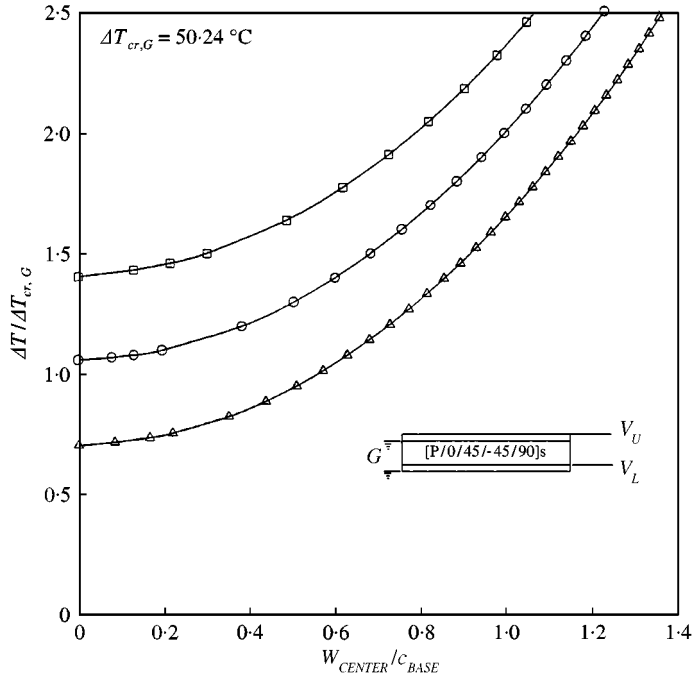

Figure 8. Active compensation for thermal buckling and postbuckling of symmetrically piezolaminated composite plate: —□—, $V_U = V_L = -100$ V; —○—, grounding ($V_U = V_L = 0$ V); —△—, $V_U = V_L = 100$ V.

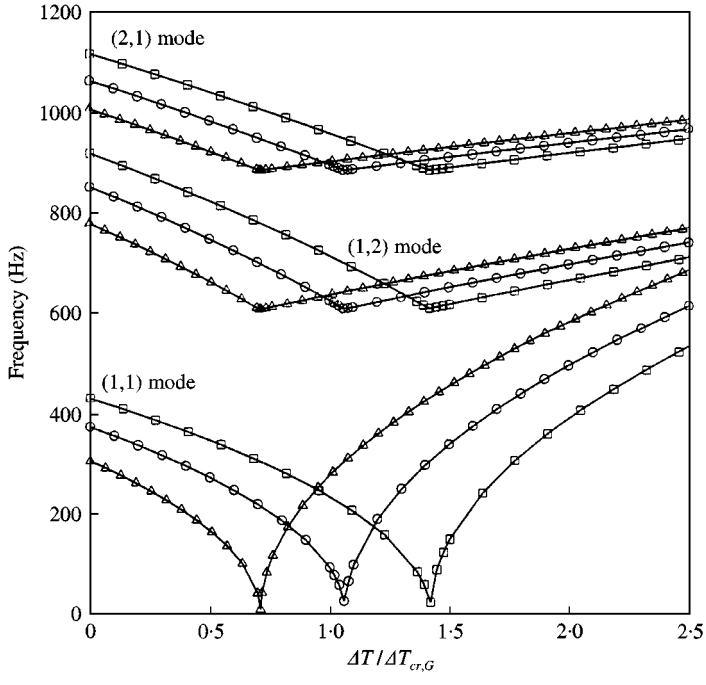

Figure 9. Vibration characteristics of symmetrically piezolaminated composite plate subject to thermal and piezoelectric loads: —□—, $V_U = V_L = -100$ V; —○—, grounding ($V_U = V_L = 0$ V); —△—, $V_U = V_L = 100$ V.

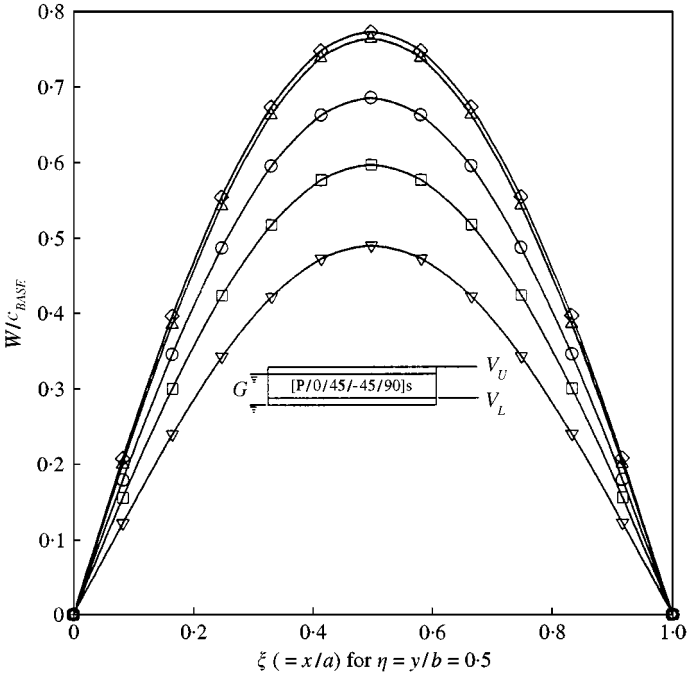

Figure 10. Thermal postbuckled deflection of symmetrically piezolaminated composite plate subject to piezoelectric force at $\Delta T/\Delta T_{cr,G} = 1{\cdot}5$: —◇—, $V_U = 30$ V, $V_L = -30$ V; —△—, $V_U = V_L = 30$ V; —○—, $V_U = V_L = 0$ V; —□—, $V_U = V_L = -30$ V; —▽—, $V_U = -30$ V, $V_L = 30$ V.

prebuckling state, the frequencies in the case of $V_U = V_L = -100$ V are higher than those in all other cases.

Several methods to suppress the thermal postbuckled deflection of the piezolaminated plate are compared in Figure 10. When a negative voltage is applied to the upper piezo-ceramic and a positive voltage is applied to the lower piezo-ceramic, the postbuckled deflection seems to be most efficiently suppressed. In other words, induced in-plane contraction force is effective in enhancing the thermal buckling load and the induced bending moment seems to be efficient in reducing the postbuckled deflection. However, the instability such as the "snap-through" phenomena is found in the bending moment control for suppressing the postbuckled deflection. Figure 11 shows this type of unstable boundary. Because of the instability phenomena, the application of excessive bending moment is not appropriate for controlling postbuckled deflections.

3.4. THERMOPIEZOELASTIC POSTBUCKLING OF AN ECCENTRICALLY PIEZOLAMINATED PLATE

The temperature field in the skin of aircraft structure has a gradient in the thickness direction. In addition, it is difficult to bond piezoelectric materials to both sides of skins. Eccentrically and partially piezolaminated composite plates can be used instead. The effective placement of the piezoceramic material is studied for the suppression of thermally buckled deflection with three configurations of piezoelectric materials: center, corner and side square patches shown in Figures 12 and 13. The lamination of active composite panel is $[(0/\pm 45/90)\mathrm{s}/P]$ and the thickness of piezoceramics is 0·2 mm. The geometry and finite

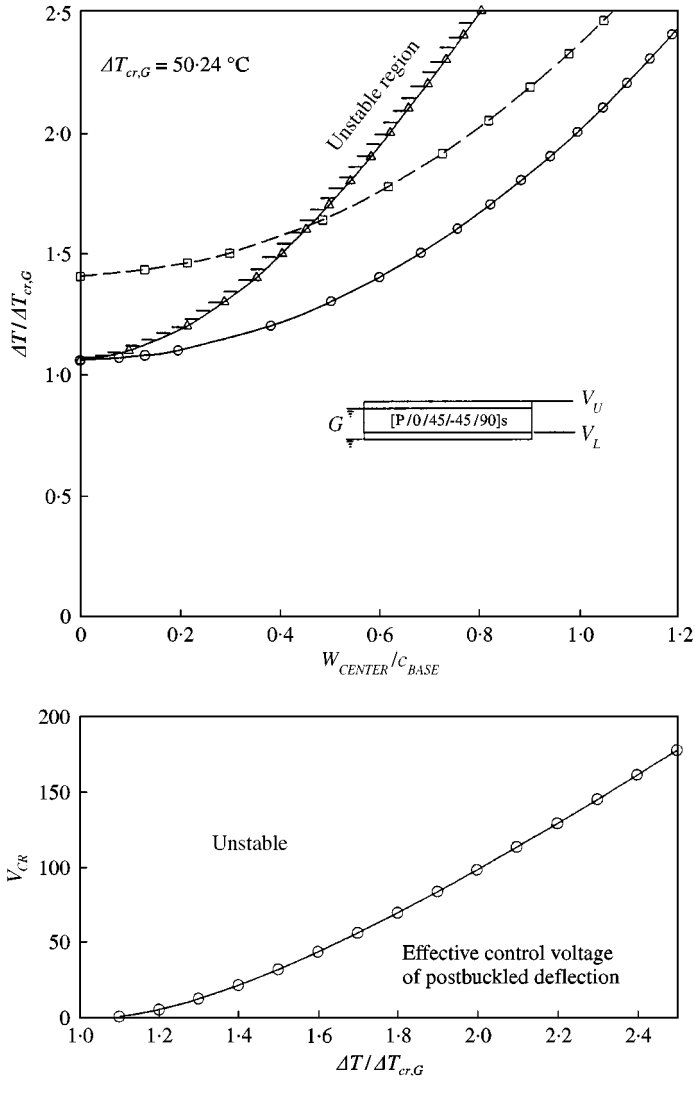

Figure 11. Unstable boundary for thermopiezoelastic postbuckling with electrically induced bending moment: —□—, $V_U = V_L = -100$ V; —○—, grounding ($V_U = V_L = 0$ V); —△—, $V_U = -V_{CR}$, $V_L = V_{CR}$.

element parameters are given as follows:

$$\text{Base composite plate geometry: } a/b = 1,\ a/c_{BASE} = 120,\ a = 120 \text{ mm}, \tag{33a}$$

$$\text{Area of piezoceramic patches: a ninth area of } S(= a * b), \tag{33b}$$

$$\text{Mesh: } 12 \times 12 \text{ with 4 node elements.} \tag{33c}$$

It is assumed that the temperature field is linear in the thickness direction and the temperature of piezoceramics is the same as that of the bottom surface of the base composite plate. The temperature gradient and mean temperature of the base composite

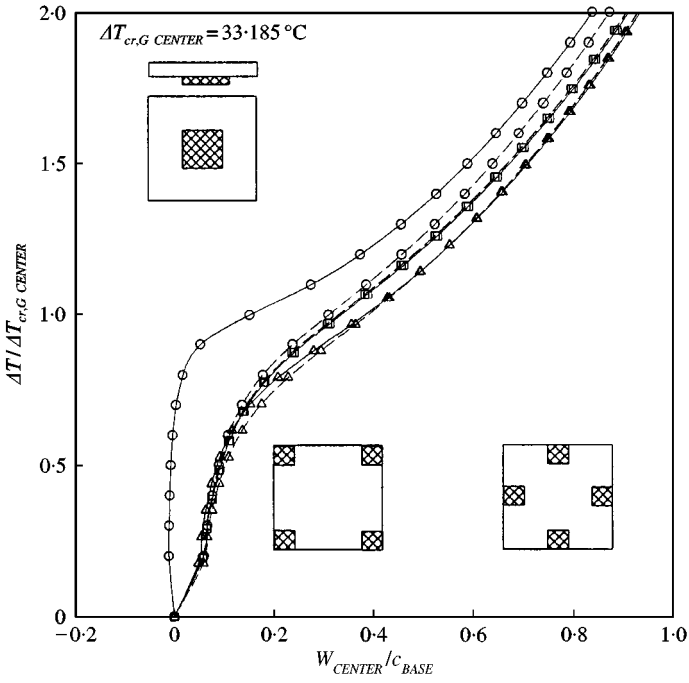

Figure 12. Thermal postbuckling of composite plate with partially bonded piezoelectric actuators: -—○—-, center ($V_L = 0$ V); —○—, center ($V_L = 100$ V); -—□—-, corner ($V_L = 0$ V); —□—, corner ($V_L = 100$ V); -—△—-, side ($V_L = 0$ V); —△—, side ($V_L = 100$ V).

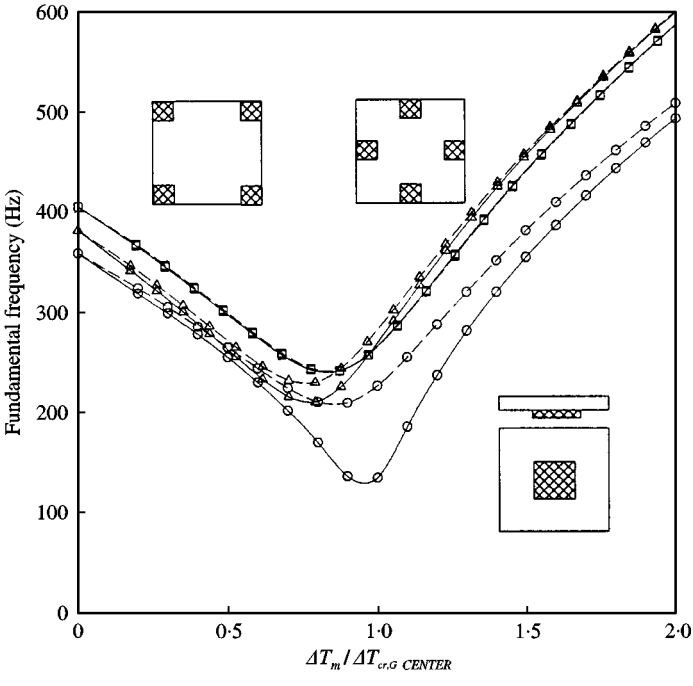

Figure 13. Effect of the configuration for piezo-ceramic on the fundamental frequency: -—□—-, corner ($V_L = 0$ V); —□—, corner ($V_L = 100$ V); -—△—-, side ($V_L = 0$ V); —△—, side ($V_L = 100$ V); -—○—-, center ($V_L = 0$ V); —○—, center ($V_L = 100$ V).

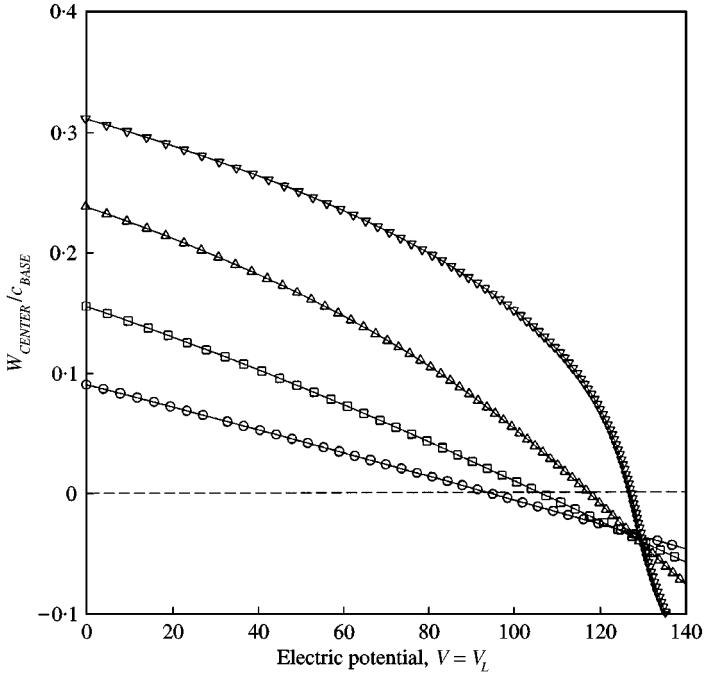

Figure 14. Suppression of a large thermal deflection of the eccentric piezolaminated plate for center patch model with thermal gradient: —○—, $\Delta T_m/\Delta T_{cr,G} = 0{\cdot}50$; —□—, $\Delta T_m/\Delta T_{cr,G} = 0{\cdot}75$; —△—, $\Delta T_m/\Delta T_{cr,G} = 0{\cdot}90$; —▽—, $\Delta T_m/\Delta T_{cr,G} = 1{\cdot}00$.

plate are defined by the temperature of the top and bottom surfaces:

$$(\Delta T^{Top\ Surface} - \Delta T^{Bottom\ Surface})/\Delta T_{cr,G} = 0{\cdot}4 \tag{34a}$$

$$\Delta T_m = (\Delta T^{Top\ Surface} + \Delta T^{Bottom\ Surface})/2 \tag{34b}$$

where $\Delta T_{cr,G}$ indicates the Euler thermal buckling temperature of each patch-type piezolaminated plate under grounding condition. Because of the thermal gradient, a thermal deflection of eccentrically piezolaminated plates is induced at even a low temperature rise. Figure 12 shows thermopiezoelastic postbuckling behavior of the plate with three kinds of actuator configurations. Here, $\Delta T_{cr,GCENTER}$ denotes the Euler thermal buckling temperature of a center-patched piezolaminated plate under grounding condition. In these cases, positive control voltage to induce tensile strain is reasonable for suppressing the thermal postbuckling with positive deflection. The case of the center patch is most effective for postbuckling control. Figure 13 shows the vibration analysis results of a composite plate with piezoelectric patches. When positive control voltage is introduced to suppress postbuckling, the fundamental frequency is decreased.

The thermopiezoelastic behavior of an eccentrically center-patched model under $\Delta T_m/\Delta T_{cr,G} \sim 0{\cdot}50, 0{\cdot}75, 0{\cdot}90, 1{\cdot}00$ is analyzed. The present results in Figure 14 show that the center-patched model can effectively suppress large thermal deflections. Figure 15 shows the thermopiezoelastic vibration characteristics. At the grounding condition, fundamental frequencies up to $\Delta T_m/\Delta T_{cr,G} = 0{\cdot}90$ are decreased but the frequency at $\Delta T_m/\Delta T_{cr,G} = 1{\cdot}0$ is slightly increased. With the increase in piezoelectric voltages, the frequencies are lowered because of the decrease in non-linear stiffness. Figure 16 shows postbuckled shapes for

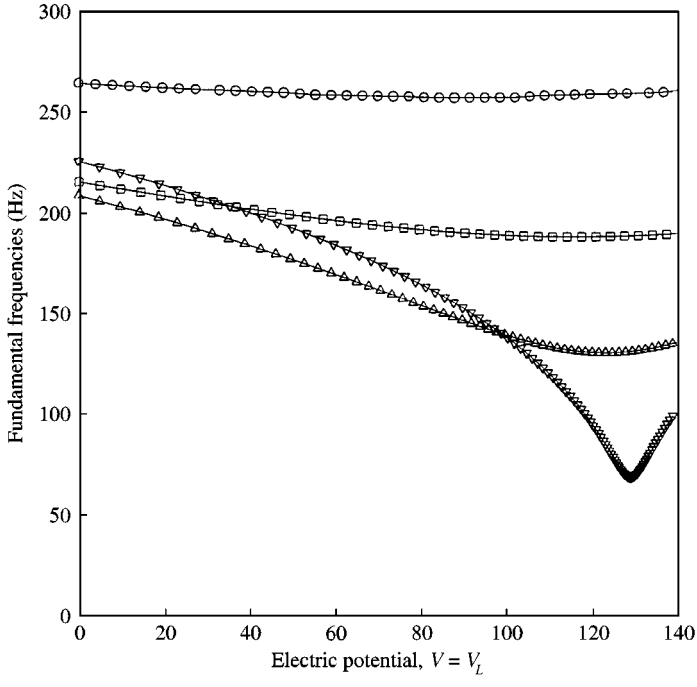

Figure 15. Vibration characteristics of eccentric piezolaminated plate for center patch model subject to piezoelectric loads: —○—, $\Delta T_m/\Delta T_{cr,G} = 0{\cdot}50$; —□—, $\Delta T_m/\Delta T_{cr,G} = 0{\cdot}75$; —△—, $\Delta T_m/\Delta T_{cr,G} = 0{\cdot}90$; —▽—, $\Delta T_m/\Delta T_{cr,G} = 1{\cdot}00$.

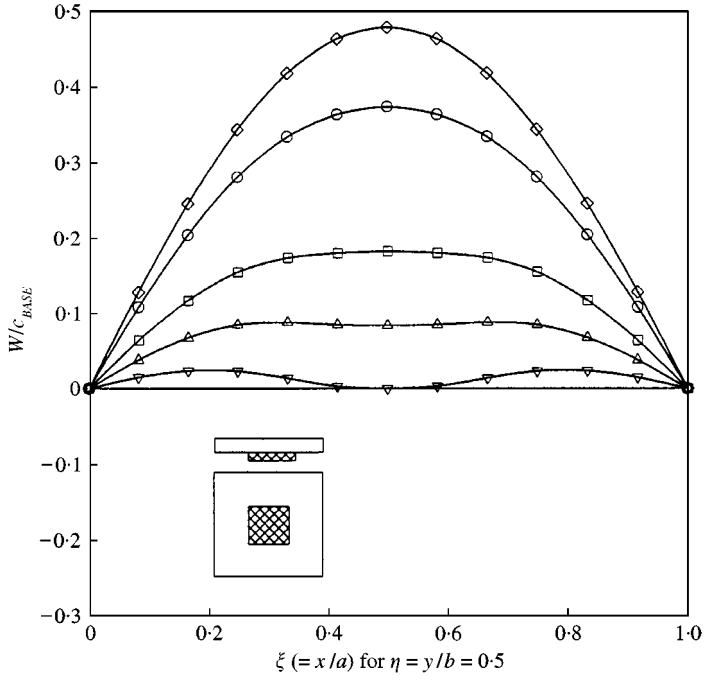

Figure 16. Suppression of postbuckled deflection of the composite plate with piezoelectric actuation at $\Delta T_m/\Delta T_{cr,G} = 1{\cdot}0$: —◇— $V_L = -100$ V; —○—, grounding ($V_L = 0$ V); —□—, $V_L = 100$ V; —△—, $V_L = 120$ V; —▽—, $V_L = 127$ V.

various control voltages at $\Delta T_m/\Delta T_{cr,G} = 1{\cdot}0$. The results in Figure 16 imply that the piezoelectric actuator partially bonded on one side of the plate can be effectively used with appropriate control voltage to reduce static deflections due to a thermal gradient.

4. CONCLUSION

Non-linear finite element equations based on the layerwise displacement theory have been developed for thermopiezoelastic analysis of laminated plates. Thermopiezoelastic postbuckling and vibration analyses have been performed for several lamination and loading types.

In the case of the symmetrically piezolaminated composite plate, only induced in-plane force is effective in enhancing the thermal buckling load, and the induced bending moment is efficient in the reduction of the postbuckled deflection within some boundaries. When the excessive control voltage for the bending moment is applied, instability like the 'snap-through' phenomena is found. These instability boundaries may be the reason why the induced bending moment is impractical for reducing postbuckled deflections.

A piezoelectric actuator partially bonded on the lower surface of the plate can be effectively used with appropriate control voltage to reduce static deflections due to a thermal gradient. Among the three configurations studied, the piezoelectric patch bonded on the central area was the most effective in the control of buckling load and postbuckled deflections. The positive control voltage which produces tensile strain is effective in the reduction of positive thermal postbuckled deflection of the plate with piezoelectric actuators partially bonded on the lower surface. However, a decrease in fundamental frequency is observed with the positive control voltage.

REFERENCES

1. T. BAILEY and J. E. HUBBARD 1985 *Journal of Guidance* **8**, 605–611. Distributed piezoelectric-polymer active vibration of a cantilever beam.
2. E. F. CRAWLEY and J. de LUIS 1987 *AIAA Journal* **25**, 1373–1385. Use of Piezoelectric actuators as elements of intelligent structures.
3. B. T. WANG and C. A. ROGERS 1991 *Journal of Computers and Materials* **25**, 433–452. Laminate plate theory for spatially distributed induced strain actuators.
4. W. S. HWANG and H. C. PARK 1993 *AIAA Journal* **31**, 930–937. Finite element modeling of piezoelectric sensors and actuators.
5. C. K. LEE 1990 *Journal of the Acoustical Society of America* **87**, 1144–1158. Theory of laminated piezoelectric plates for the design of distributed sensors/actuators. Part I: governing equations and reciprocal relationships.
6. J. H. HAN and I. LEE 1997 *Journal of Intelligent Material Systems and Structures* **8**, 249–259. Active damping enhancement of composite plates with electrode designed piezoelectric materials.
7. H. S. TZOU and M. GADRE 1989 *Journal of Sound and Vibration* **132**, 433–450. Theoretical analysis of a multi-layered thin shell coupled with piezoelectric shell actuators for distributed vibration controls.
8. H. S. TZOU and C. I. TSENG 1990 *Journal of Sound and Vibration* **138**, 17–34. Distributed piezoelectric sensor/actuator design for dynamic measurement/control of distributed parameter systems: a piezoelectric finite element approach.
9. D. H. ROBBINS and J. N. REDDY 1991 *Computers and Structures* **41**, 265–279. Analysis of piezoelectrically actuated beams using a layerwise displacement theory.
10. D. A. SARAVANOS and P. R. HEYLIGER 1995 *Journal of Intelligent Material Systems and Structures* **6**, 350–363. Coupled layerwise analysis of composite beams with embedded piezoelectric sensors and actuators.
11. J. H. HAN and I. LEE 1998 *Composite Part B*: *Engineering* **29**, *Issue* 5, 621–632. Analysis of composite plates with piezoelectric actuators for vibration control using layerwise displacement theory.

12. D. M. Lee and I. Lee 1997 *Computers & Structures* **63**, 371–378. Vibration behavior of thermally postbuckled anisotropic plates using first order shear deformable plate theory.
13. E. J. Barbero and J. N. Reddy 1994 *AIAA Journal* **28**, 1987–1994. Nonlinear analysis of composite laminates using a generalized laminated plate theory.
14. P. F. Pai, A. H. Nayfeh, K. Oh and D. T. Mook 1993 *Journal of Solids and Structures* **30**, 1603–1630. A refined nonlinear model of piezoelectric plates.
15. H. S. Tzou and R. Ye 1994 *Journal of Vibration and Acoustics* **116**, 489–495. Piezothermoelasticity and precision contol of piezoelectric systems: theory and finite element analysis.
16. H. S. Tzou and Y. H. Zhou 1997 *Journal of Vibration and Acoustics* **119**, 382–389. Nonlinear piezothermoelasticity and multi-field actuators, Part 2: control of nonlinear deflection, buckling and dynamics.
17. Y. Bao, H. S. Tzou and V. B. Venkayya 1998 *Journal of Sound and Vibration* **209**, 505–518. Analysis of nonlinear piezothermoelastic laminated beams with electric and temperature effects.
18. H. J. Lee and D. A. Saravanos 1997 *International Journal of Solids Structures* **34**, 3355–3371. Generalized finite element formulation for smart multilayered thermal piezoelectric composite plates.
19. R. M. S. Gowda and K. A. V. Pandalai 1970 In *Studies in Structural Mechanics* (K. A. V. Pandalai, editor) , IIT, Madras, 9–44. Thermal buckling of orthotropic plates.
20. K. R. Thangaratnam, Palaninathan and J. Ramachandran 1989 *Computers & Structures* **32**, 1117–1124. Thermal buckling of composite laminated plates.
21. R. C. Averil and J. N. Reddy 1993 *Proceedings of AIAA/ASME/ASCE/AHS/ASC/34th SDM Conference* AIAA-93-1337-CP, 315–360. Thermomechanical postbuckling analysis of laminated composite shells.

APPENDIX A: NOMENCLATURE

a, b	panel length, width
c	total thickness of the plate
c_{BASE}	thickness of the base plates
σ_i	stress
ε_j	strain
E_k	electric field
D_k	electric displacement
ΔT_k	temperature rise in kth layer
$Q_{ij}^{E,\Delta T}$	elastic moduli
$\varepsilon_{kl}^{S,\Delta T}$	dielectric constant
e_{kj}	piezoelectric coefficient
$\alpha_i^{S,E}$	thermal expansion coefficient
$p_k^{S,E}$	temperature stress coefficient
$\Phi^J(z)$	Lagrangian interpolation function

Subscripts

S	transverse shear properties
e	finite element
U	upper piezo-actuator
L	lower piezo-actuator
G	grounding